Envelope Correlation Coefficient of a Two-Port MIMO Terminal Antenna under Uniform and Gaussian Angular Power Spectrum with User's Hand Effect

Ahmed M. Elshirkasi[1], Azremi Abdullah Al-Hadi[1, *], Mohd F. Mansor[2], Rizwan Khan[1], and Ping J. Soh[1]

Abstract—This paper studies the effects of incident wave angular power spectrum (APS) distribution and user hand effect on the envelope correlation coefficient (ECC) of a two-port MIMO antenna operating in the sub 6 GHz LTE-U frequency band. APS of uniform and Gaussian distributions are used with different Gaussian angular spread (AS) values, i.e., 10°, 30°, 50°, and 70°. A prototype was fabricated, and three-dimensional radiation patterns of the antenna elements were measured in an anechoic chamber from 4 to 6 GHz in both cases of free space and when the prototype is held in data mode using a hand phantom. An algorithm to calculate ECC from the complex data of far field radiation pattern with different APS distributions is explained in detail. Results show that user hand presence increases ECC between ports compared with free space, whose increase is more obvious under Gaussian APS. ECC values under uniform APS is practically zero over the entire frequency range except at frequencies close to 6 GHz, where the highest ECC values are 0.13 and 0.16 in free space and with user hand, respectively. However, Gaussian APS with different ASs shows a significant impact of the ECC. With narrow AS of 10°, ECC at some incident directions can be as high as 0.84 (in free space) and 0.92 (with user hand), and the mean ECC values under this AS are 0.25 (in free space) and 0.37 (with user hand). ECC values keep decreasing as AS gets wider, with the maximum ECC at AS = 70° observed to be 0.23 and 0.34 in free space and with user hand, respectively, whereas the mean ECC values are close to uniform APS. Statistical distribution of the ECC showed good agreement with exponential distribution, with a better agreement between measured ECC and exponential distribution observed in free space with wider AS.

1. INTRODUCTION

One of the main key design components to realize high data rates in modern wireless communication systems is MIMO antennas [1, 2]. These MIMO antennas should have low correlation between their ports and high total efficiency of ports [3]. Performance evaluation of MIMO antennas is an essential step to design an efficient MIMO link. However, an important aspect when evaluating the performance of the MIMO antennas in mobile communication is the effects of user's hand and body [4]. These effects cause degradation in the system performance by different ways such as changing the impedance matching and radiation pattern. Moreover, user's hand and body reduce the amount of radiated power due to absorption by the body tissue. They can also shift the resonant frequency and operating bandwidth of the antenna [3, 5, 6]. In [7] a review is provided about the effect of user's body on mobile terminal antennas and discusses several proposed techniques in the literature to mitigate this effect.

Many of the performance evaluations of MIMO antenna designs in the literature are performed under the assumption of a uniform APS, for example [8–10]. The signal is assumed to arrive equally from all directions. However, APS distributions in real propagation environments are often modeled with narrower distributions, assuming that the incident signals are coming from specific directions with limited AS [11, 12]. Besides the uniform distribution, other models such as the Gaussian and Laplacian distributions have been proposed in literature [13–15]. These models can be used to control the incident power from predefined directions and predefined angular spreads. In this paper, a uniform and Gaussian APS were used in the post processing of measured far field radiation pattern data to calculate ECC between the two ports in free space and with user hand grip in data mode. Details of the ECC calculation will be presented in the following sections.

This paper is organized as follows. Section 2 presents the different methods for calculating envelop correlation coefficient, with a discussion on the advantages and disadvantages of each method. Section 3 presents a detailed algorithm to construct the APS distribution and calculate ECC from the complex data of the far-field radiation patterns. Section 4 introduces the two port MIMO antenna design, fabrication, and detailed measurement results. Section 5 discusses the results prior to the conclusions in Section 6.

2. ENVELOPE CORRELATION COEFFICIENT (ECC)

Envelope correlation coefficient is a main metric when designing MIMO antennas for mobile communications [11]. It characterizes the correlation between every two ports. MIMO antennas should have low ECC to indicate that channels are independent, and hence the system provides a high diversity gain (DG) and high capacity [16]. The ECC between ports i and $j \rho_{e,ij}$ can be calculated from S-parameters. This formula was presented in [17] for two ports only, and it was generalized for any number of ports n in [18] as follows:

$$\rho_{e,ij} = \left| \frac{-\sum_{n=1}^{N} S_{ni}^* S_{nj}}{\sqrt{\left(1 - \sum_{n=1}^{N} |S_{ni}|^2\right)\left(1 - \sum_{n=1}^{N} |S_{nj}|^2\right)}} \right|^2 \tag{1}$$

where S_{ni} and S_{nj} are the S-parameters between ports i and j and the other ports of the system. This formula is used due to its simplicity, as S-parameters can be measured easily. However, this formula is only accurate if the total radiation efficiency of antenna elements is 100%, which is unrealistic in practice [16]. A modified version of this formula that takes into account the non-ideal radiation efficiency of ports was proposed for two ports in [19], and its generalization for any number of ports n is derived in [16] as follows:

$$\rho_{e,ij} = \left| \frac{-\sum_{n=1}^{N} S_{ni}^* S_{nj}}{\sqrt{\left(1 - \sum_{n=1}^{N} |S_{ni}|^2\right)\left(1 - \sum_{n=1}^{N} |S_{nj}|^2\right)} \eta_{rad,i}\eta_{rad,j}} + \sqrt{\left(\frac{1}{\eta_{rad,i}} - 1\right)\left(\frac{1}{\eta_{rad,j}} - 1\right)} \right|^2 \tag{2}$$

where $\eta_{rad,i}$ and $\eta_{rad,j}$ are the radiation efficiencies of ports i and j, respectively. Including the efficiencies improves the calculation accuracy of the envelope correlation coefficient. However, this accuracy improvement works only for antenna ports with efficiencies larger than 60%, which otherwise may result in significant calculation errors [16]. Moreover, besides the ports efficiency considerations in both S-parameter methods, these two methods assume a uniform APS only and does not consider the directive APS distributions.

The method that overcomes the disadvantages of both S-parameter methods and provides accurate results is to calculate ECC from the complex data of the three-dimensional far-field radiation patterns.

This can be performed via the integral relation of ECC as follows [20]:

$$\rho_{e,ij} = \left| \frac{\int_0^{2\pi} \int_0^{\pi} \left(\text{XPR} \cdot E_{\theta i} \cdot E_{\theta j}^* \cdot P_\theta + \text{XPR} \cdot E_{\phi i} \cdot E_{\phi j}^* \cdot P_\phi \right) \sin(\theta) d\theta d\phi}{\sqrt{\prod_{k=i,j} \int_0^{2\pi} \int_0^{\pi} \left(\text{XPR} \cdot E_{\theta k} \cdot E_{\theta k}^* \cdot P_\theta + \text{XPR} \cdot E_{\phi k} \cdot E_{\phi k}^* \cdot P_\phi \right) \sin(\theta) d\theta d\phi}} \right|^2 \tag{3}$$

where $\text{XPR} = P_V/P_H$ is the cross discrimination ratio between vertical and horizontal polarized power components, and $E_{\theta i}$, $E_{\theta j}$, $E_{\phi i}$, $E_{\phi j}$ are the field components of i and j ports in elevation and azimuth directions, respectively. P_θ and P_ϕ are the elevational and azimuthal APS distribution which should satisfy the following normalization condition:

$$\int_0^{2\pi} \int_0^{\pi} P_\theta \cdot \sin(\theta) \, d\theta d\phi = 1, \quad \int_0^{2\pi} \int_0^{\pi} P_\phi \cdot \sin(\theta) \, d\theta d\phi = 1 \tag{4}$$

Equation (3) provides the most accurate result of ECC, whereas other equations should be avoided [16]. However, this equation requires the complex data of far-field radiation pattern of the antenna ports, which needs to be measured in an anechoic chamber. This may not be easily available, especially if the user body effect needs to be included in the study. In such cases, the anechoic chamber should be able to accommodate a human volunteer, or at least phantoms of human head and hands. In addition to that, a computer program is needed to post process the data and calculate the integrals in Equation (3) numerically.

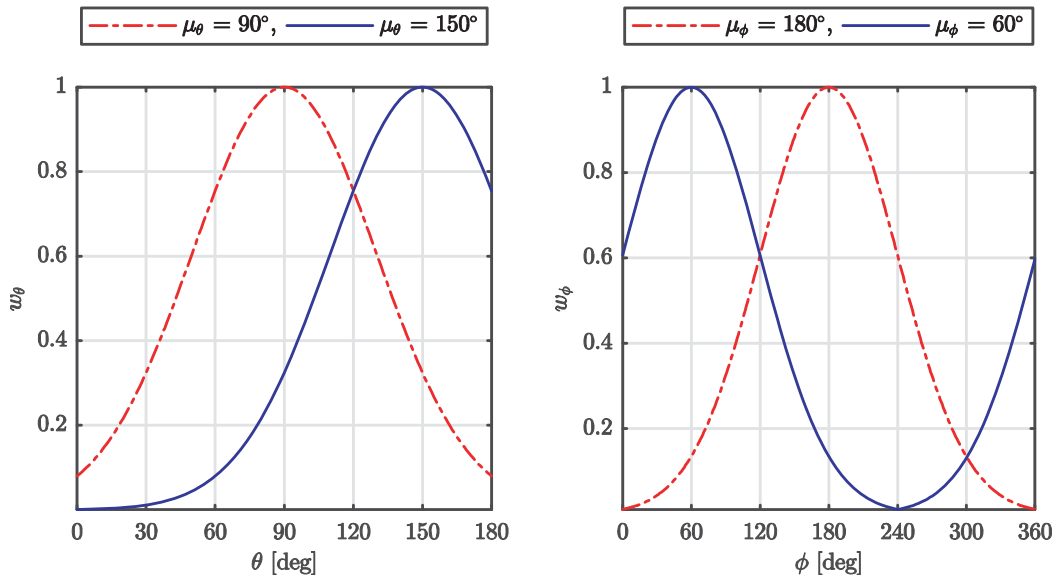The two models of APS distributions studied in this paper are described below [21, 22]:

1- Uniform in both elevation and azimuth:

$$P_\theta(\theta\phi) = P_\phi(\theta\phi) = 1/4\pi$$
$$0 \le \theta < \pi, \quad 0 \le \phi < 2\pi \tag{5}$$

The constant value of $1/4\pi$ results from the condition of Equation (4).

2- Gaussian in Azimuth, Gaussian in elevation:

$$P_\theta(\theta, \phi) = P_\phi(\theta, \phi) = A_0 w_\theta w_\phi = A_0 \exp\left(-\frac{(\theta - \mu_\theta)^2}{2\sigma_\theta^2} \right) \exp\left(-\frac{(\phi - \mu_\phi)^2}{2\sigma_\phi^2} \right) \tag{6}$$

$$0 \le \theta < \pi, \quad 0 \le \phi < 2\pi$$

Figure 1. Gaussian distribution in elevation and azimuth direction (cyclically shifted in azimuth).

where μ_θ, σ_θ, μ_ϕ, and σ_ϕ are the mean values and standard deviations of the Gaussian distributions in elevation and azimuth directions, respectively. A_0 is a scaling constant to fulfill the normalization condition of Equation (4). Note that the Gaussian curve of w_ϕ in Equation (6) is cyclically shifted around the mean value within the closed interval of ϕ between 0 and 2π. The cyclic shift process of the Gaussian curve with different mean values is illustrated in Figure 1.

Standard deviation values of Gaussian distributions in Equation (6) represent AS of the incoming signal. In measurement-based WINNER II wireless channel model, the angular spread at the user device is found between $12°$ and $53°$, depending on the propagation scenario [23]. In [12] a standard deviation of $30°$ is used for Gaussian APS in both elevation and azimuth directions. In [24] the capacity of a two port MIMO is studied under Gaussian APS of different standard deviations namely $15°$, $30°$ and $60°$. Each one of these values is used for both elevation and azimuth directions respectively. In [25], standard deviation values of $40°$ and $60°$ in elevation and azimuth respectively are used. In this paper, four cases with standard elevation values of $10°$, $30°$, $50°$, and $70°$ are studied, with each value used in both elevation and azimuth components of the Gaussian distribution. To change the incident wave directions, the elevation-azimuth plane is divided into discrete points with a step size of $10°$ in each direction, and each pair of these discrete angles represents the mean values (μ_θ, μ_ϕ) of the two Gaussian distributions of the APS.

3. NUMERICAL APPROXIMATION OF ECC EQUATION

This section presents details of the numerical method to approximate the double integrals in Equation (3) so that a computer program can be written to perform this calculation. The far-field radiation pattern of each antenna element is simulated or measured at discreet angles along elevation and azimuth coordinate system. Let θ_0, θ_1, $\ldots$, $\theta_{n_\theta-1}$ and ϕ_0, ϕ_1, $\ldots,$, $\phi_{n_\phi-1}$ be the discrete angles in elevation and azimuth directions over the intervals from 0 to π and from 0 to 2π, respectively. Each measured or simulated field component in Equation (3) at these angles can be arranged in a matrix of size $n_\theta \times n_\phi$. For example $E_{\theta i}$ component is presented as:

$$\mathbf{E}_{\theta_i} = \begin{bmatrix} E_{\theta i}^{\theta_0,\phi_0} & E_{\theta i}^{\theta_0,\phi_1} & \ldots & E_{\theta i}^{\theta_0,\phi_{n_\phi-1}} \\ E_{\theta i}^{\theta_1,\phi_0} & E_{\theta i}^{\theta_1,\phi_1} & \ldots & E_{\theta i}^{\theta_2,\phi_{n_\phi-1}} \\ \vdots & \vdots & \ldots & \vdots \\ E_{\theta i}^{\theta_{n_\theta-1},\phi_0} & E_{\theta i}^{\theta_{n_\theta-1},\phi_1} & \ldots & E_{\theta i}^{\theta_{n_\theta-1},\phi_{n_\phi-1}} \end{bmatrix} \tag{7}$$

Other components, i.e., $E_{\theta j}$, $E_{\phi i}$ and $E_{\phi j}$, are represented in the same way at all combinations of θ and ϕ angles. Each Gaussian component of the APS can be represented as a column vector of the form:

$$\mathbf{w}_\theta = \begin{bmatrix} w_\theta^{\theta_0} & w_\theta^{\theta_1} & \ldots & w_\theta^{\theta_{n_\theta-1}} \end{bmatrix}^T, \quad \mathbf{w}_\phi = \begin{bmatrix} w_\phi^{\phi_0} & w_\phi^{\phi_1} & \ldots & w_\phi^{\theta_{n_\phi-1}} \end{bmatrix}^T, \tag{8}$$

and the APS matrix is formed as follows:

$$\mathbf{P}_\theta = \mathbf{P}_\phi = A_0 \mathbf{w}_\theta \mathbf{w}_\phi^T \tag{9}$$

The approximated discrete version of the integral in Equation (3) can then be written as [21]:

$$\rho_{e,ij} =$$

$$\left| \frac{\displaystyle\sum_{m=0}^{n_\theta-1}\sum_{n=0}^{n_\phi-1}\left(\mathrm{XPR}\cdot\mathbf{E}_{\theta i}^{m,n}\cdot\left(\mathbf{E}_{\theta j}^{m,n}\right)^*\cdot\mathbf{P}_\theta^{m,n}+\mathrm{XPR}\cdot\mathbf{E}_{\phi i}^{m,n}\cdot\left(\mathbf{E}_{\phi j}^{m,n}\right)^*\cdot\mathbf{P}_\phi^{m,n}\right)\cdot\sin\left(\theta^m\right)\cdot\Delta\theta\cdot\Delta\phi}{\sqrt{\displaystyle\prod_{k=i,j}\sum_{m=0}^{n_\theta-1}\sum_{n=0}^{n_\phi-1}\left(\mathrm{XPR}\cdot\mathbf{E}_{\theta k}^{m,n}\cdot\left(\mathbf{E}_{\theta k}^{m,n}\right)^*\cdot\mathbf{P}_\theta^{m,n}+\mathrm{XPR}\cdot\mathbf{E}_{\phi k}^{m,n}\cdot\left(\mathbf{E}_{\phi k}^{m,n}\right)^*\cdot\mathbf{P}_\phi^{m,n}\right)\cdot\sin\left(\theta^m\right)\cdot\Delta\theta\cdot\Delta\phi}} \right|^2$$

$$\tag{10}$$

where $\Delta\theta$ and $\Delta\phi$ are the step sizes at the elevation and azimuth directions, respectively, both in simulations and measurements (in radian). Equation (10) is the required relation to calculate ECC.

A computer program in Matlab or other programming languages can be written to process far-field radiation pattern data of MIMO antenna ports and produce ECC values.

To show the accuracy of the approximation in Equation (10), simulated far-field radiation pattern data from the two ports were exported from CST Microwave Studio and processed with Matlab under different incident wave directions, according to the numerical approximation in this section. The ECC results from Matlab code are compared with ECC results generated by CST. Figure 2 shows a good agreement between them.
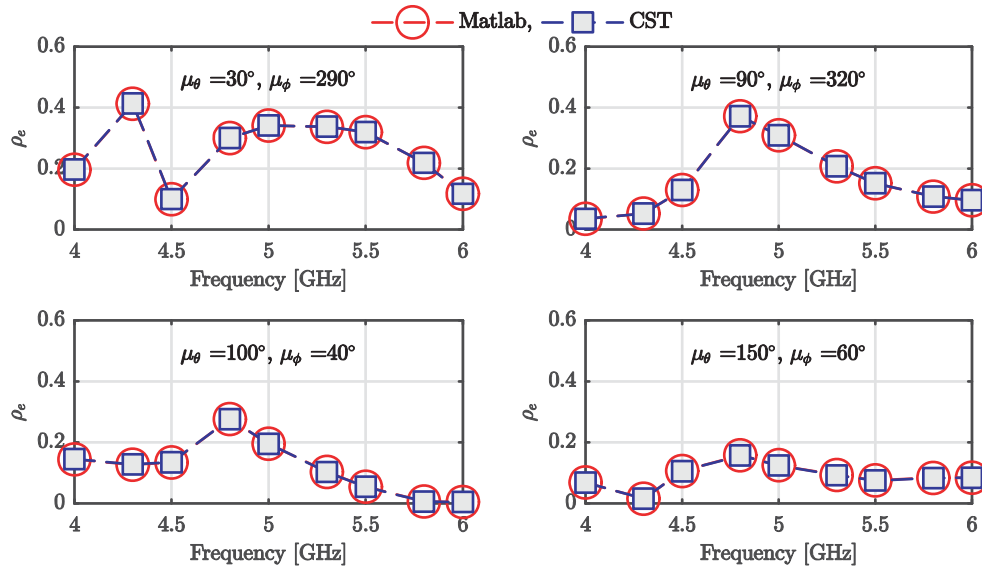
Figure 2. Comparison between ECC calculation from CST and numerical approximation in Equation (10).

4. MIMO ANTENNAS DESIGN AND MEASUREMENT

The two-port MIMO antenna has been designed and simulated in CST Microwave Studio prior to its prototyping and measurements of its complex far-field radiation pattern in an anechoic chamber.
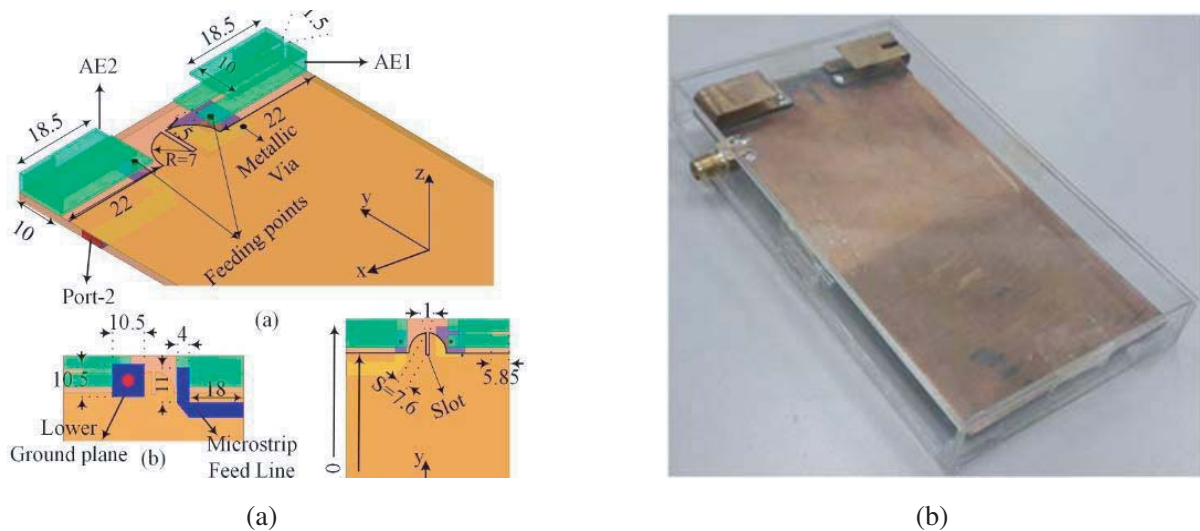
Figure 3. (a) Details of the two ports placed on top of the device. (b) Prototype inside a methacrylate box.

Measurement was performed in free space and when a hand phantom grips the prototype. Figure 3 shows the details of the two ports (a) and the fabricated prototype of antenna (b).

Measurement was carried out in an anechoic chamber of the Advanced Communication Engineering


(a)

(b)

(c)

(d)

(e)

(f)
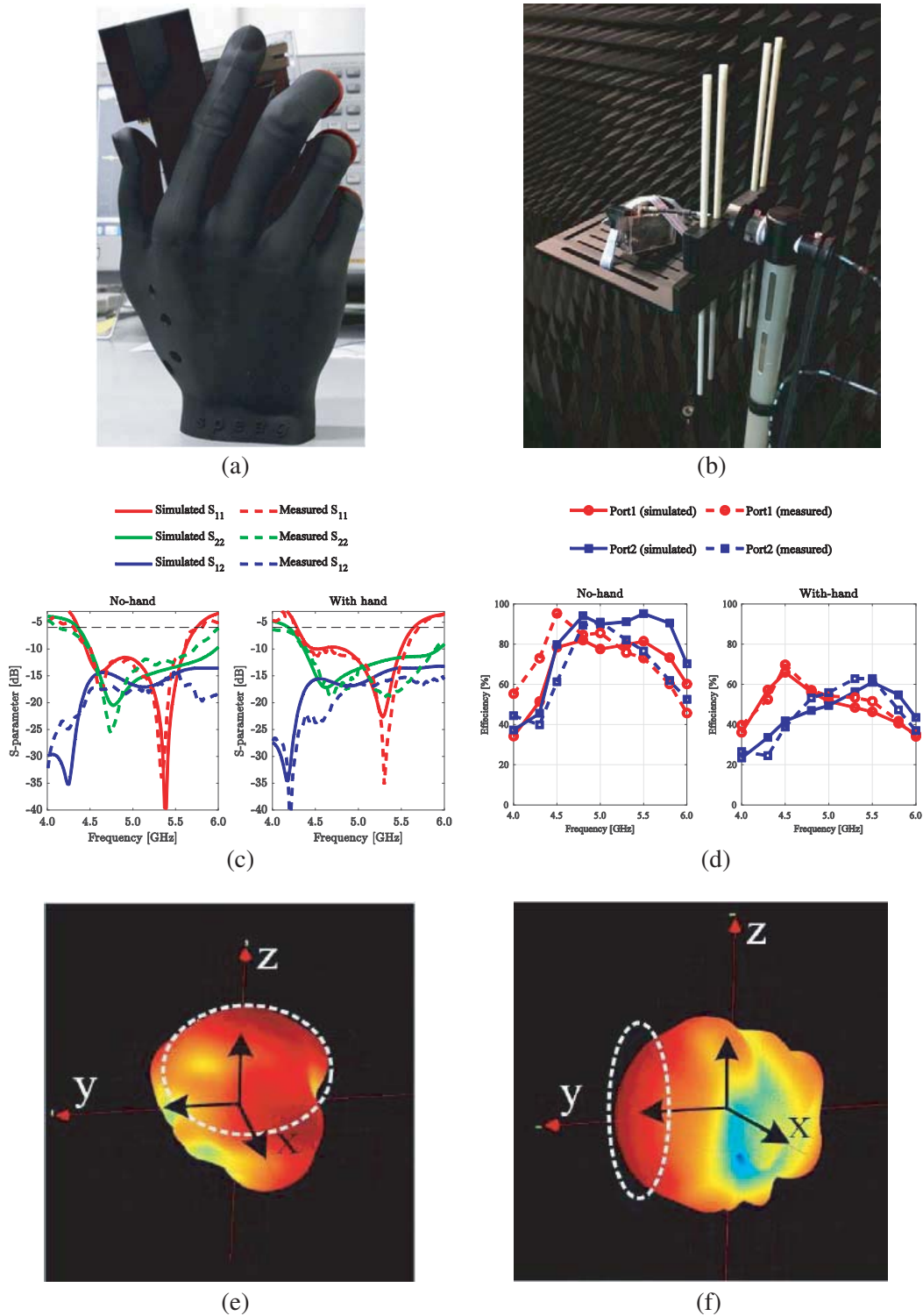
Figure 4. (a) Prototype gripped hand phantom. (b) Far-field radiation pattern of the antenna elements being measured in the anechoic chamber. (c) Simulated and measured S-parameter. (d) Simulated and measured efficiency. (e) and (f) Free space measured 3D radiation pattern of ports 1 and 2 at 5.3 GHz.

Center (ACE) in School of Computer and Communication Engineering (SCCE) at University Malaysia Perlis (UNIMAP), Perlis city, Malaysia. The measurement step size is 5 degrees in both elevation and azimuth directions with measurement range from 4 to 6 GHz. Figure 4(a) shows the prototype held in the hand phantom, whereas Figure 4(b) shows the radiation pattern measurement setup inside the anechoic chamber. Figure 4(c) and (d) show simulated and measured S-parameters and efficiencies, respectively, whereas 4(e) and (f) show the measured radiation pattern of the ports in free space at 5.3 GHz.

5. RESULTS AND DISCUSSION

ECC results calculated from simulations and measurements in a uniform environment are shown in Figure 5. Simulation and measurement results without and with user hand follow the same behavior and show a good agreement. ECC is close to zero over the entire frequency range except for the edge frequency values of 5.8 GHz and 6 GHz, where ECC values are higher. The maximum ECC values which
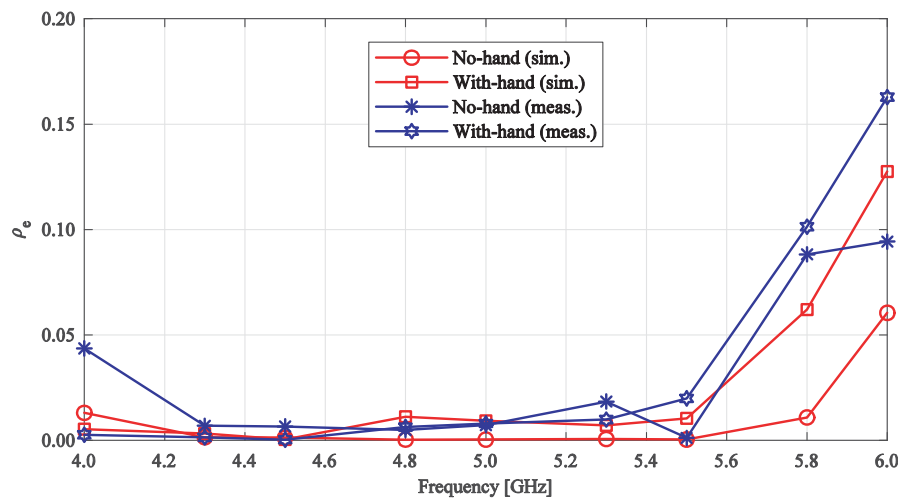
Figure 5. ECC values in a uniform environment calculated from simulation and measurement radiation pattern data.

Table 1. ECC of the two-port MIMO antenna in free space and with user's hand. All results are under uniform APS.

Reference	Frequency	ECC (less than)	
		Without hand	With hand/body effect
[3]	698–990 MHz	0.8	0.7
	1710–5530 MHz	0.05	0.12
[8]	GSM850/900/1800/1900, UMTS2100, and LTE2300/2500	0.4	-
[26]	2.4 GHz–2.5 GHz (ISM band)	0.1	0.1 (body effect)
[27]	2.3–2.8 GHz	0.28	-
	4.8–5.7 GHz	0.25	-
[28]	1430–2690 MHz	0.27	0.3
This paper	4–6 GHz	0.06 (simulated) 0.09 (measured)	0.13 (simulated) 0.16 (measured)
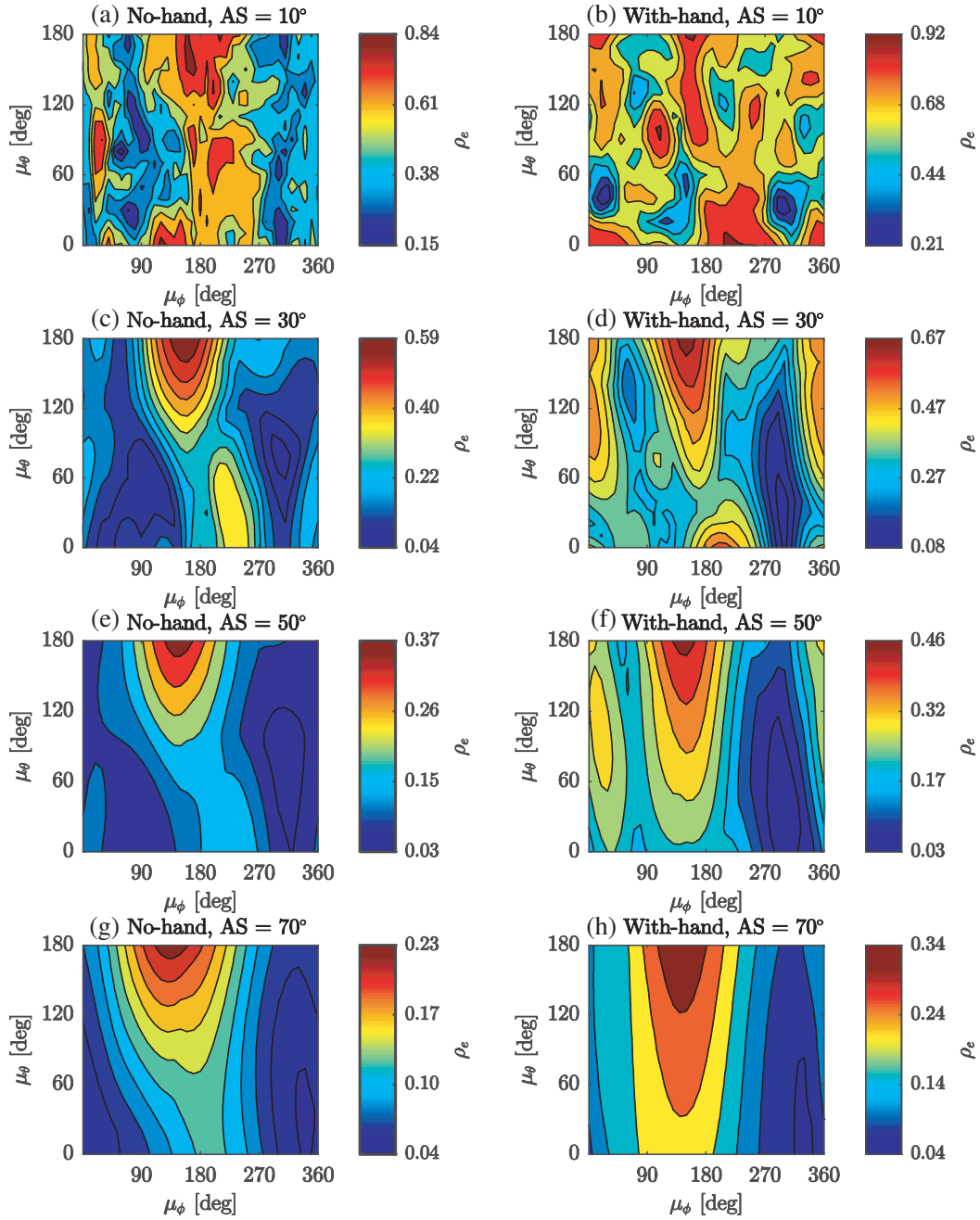
Figure 6. Maximum ECC at every incident wave direction with different AS values for the cases of without and with user's hand.

occur at 6 GHz are listed in Table 1 and compared with other values obtained from two-port MIMO antennas in literature.

For brevity reason, only measurement data will be presented in the rest of this paper.

Figure 6 shows the calculated ECC results according to the numerical approximation in Equation (10) with Gaussian APS. The figure shows the maximum ECC value in the frequency range at every incident direction in the elevation-azimuth grid with different AS values. In addition to that, these results are shown for both cases without and with user's hand.

In general, the presence of user's hand leads to increased ECC range, as well as the number of incident directions that produce higher ECC values within this range. Besides that, it is also observed

that a narrow AS produces higher ECC. In panels (a) and (b) of AS of 10°, ECC ranges between 0.15 and 0.84 for the case without user's hand. However, this range is increased due to the effects of the user's hand between 0.21 and 0.92, with more incident directions giving high ECC values within this range. In panels (c) and (d) with AS of 30°, the ECC range dropped to between 0.04 and 0.59 without user's hand, and between 0.08 and 0.67 with user's hand. Further improvement in ECC is obtained as AS gets wider. In panels (e) and (f) with AS of 50°, ECC ranges between 0.03 and 0.37 without user's hand and between 0.03 and 0.46 with user's hand. In panels (g) and (h), with AS of 70°, the least ECC range is obtained, and most directions produce ECC values close to a uniform environment. ECC with this AS value ranges between 0.04 and 0.23, and between 0.04 and 0.34, without and with user hand,
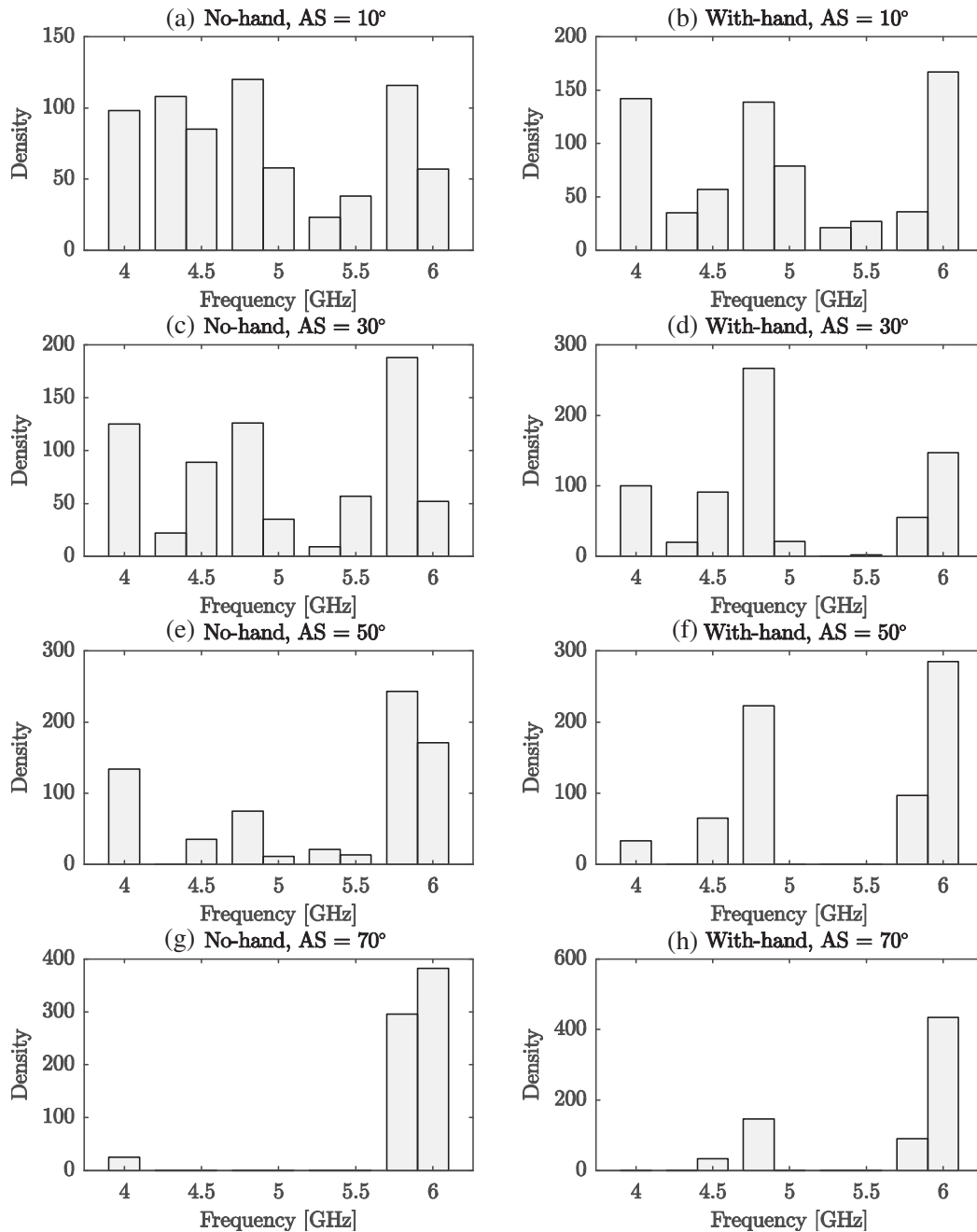
Figure 7. Distribution of frequencies that provides a maximum ECC at every incident direction for the cases of without and with user's hand.

respectively. It can also be noticed that higher ECC values originates from a certain spot within each AS value. This spot is when μ_θ is from 120° to 180° and μ_ϕ from 100° to 160°. ECC drops significantly outside this spot for each AS value.

In the same context of analyzing maximum ECC at every incident direction, corresponding frequencies that produced these maximum ECC values have been studied, and results are shown in Figure 7. It can be noticed that at AS values of 10°, 30°, and 50°, all frequencies within the measurement range have a contribution in producing maximum ECC values. However, this is not the case when AS gets wider, i.e., 70° where edge frequencies are responsible for producing maximum ECC with more
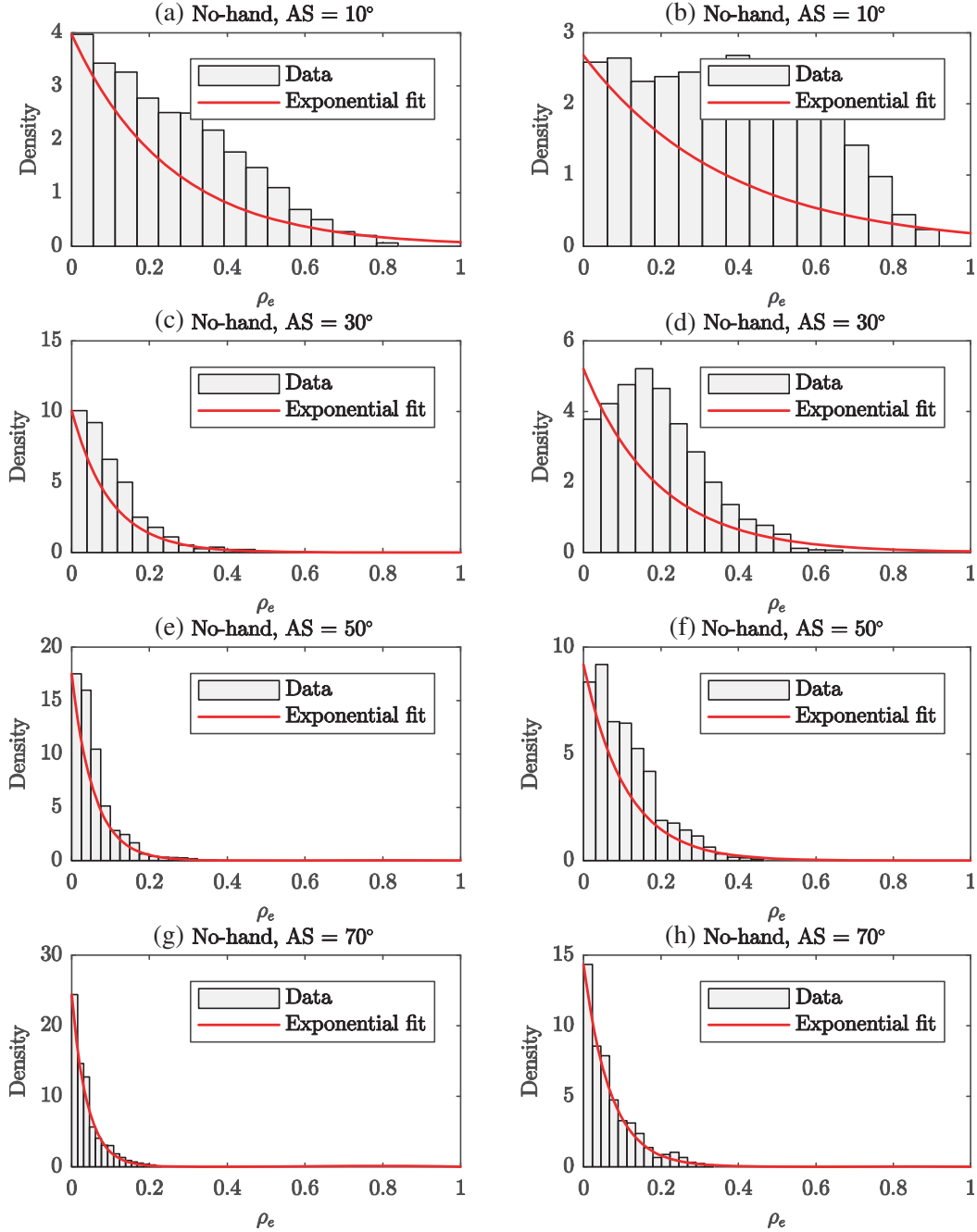
Figure 8. Exponential fit with ECC under different AS values for the cases of without and with user's hand.

contribution from left edge frequencies namely 5.8 GHz and 6 GHz. This result is in accordance with ECC results in uniform environment illustrated in Figure 5 where higher ECC values are at edge frequencies.

Results in Figures 6 and 7 indicate that at AS = 70° the Gaussian environment gives results close to uniform environments and with AS less than 70° results are different between uniform and Gaussian. This difference gets bigger at smaller AS values of the incident wave.

Results in Figures 6 and 7 show the maximum ECC values and corresponding frequencies at every incident direction. The following analysis takes all ECC values into consideration (not only maximum ECC) from all frequency values and all incident directions. The total number of ECC values in this case is $n_{\text{ECC}} = n_f \cdot n_\theta \cdot n_\phi$ where n_f, n_θ and n_ϕ are the numbers of points in the frequency range, and elevation and azimuth directions, respectively.
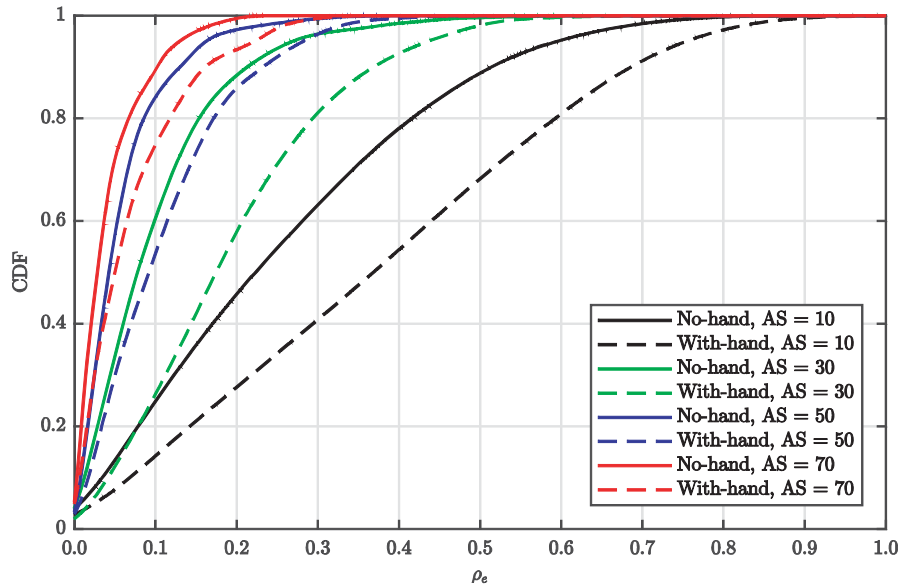
Figure 9. CDF curves of ECC with different AS values for the cases of without and with user's hand.
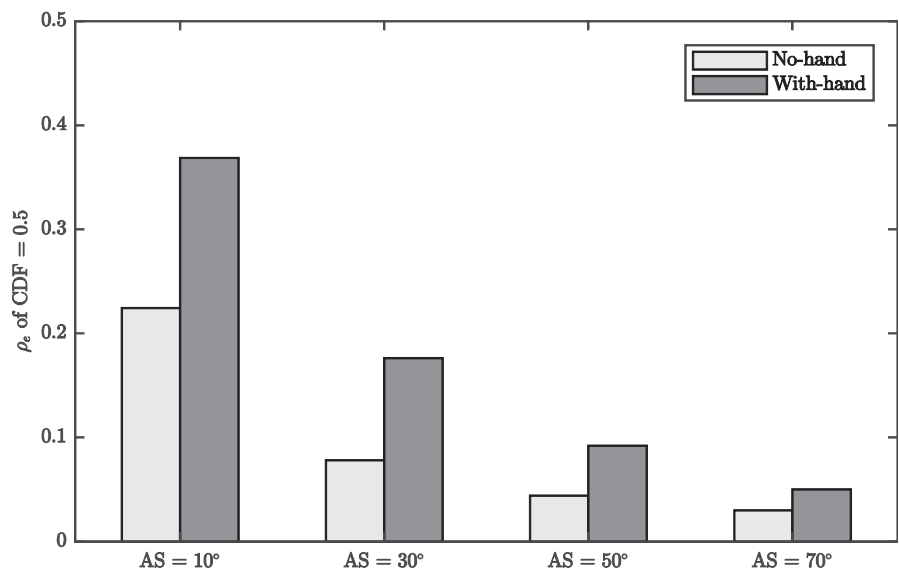
Figure 10. ECC at 0.5-horizontal level of CDF curves of Figure 9 with different AS values for the cases of without and with user's hand.

Figure 8 shows the statistical distribution of these ECC values with different ASs for the cases without and with user's hand effect.

Fitting the results shows good agreement between measured ECC and exponential distribution whose equation is given by:

$$f(x) = \frac{1}{\mu} e^{-\frac{x}{\mu}} \tag{11}$$

where μ is the mean value of the distribution. It can be noticed that the agreement between ECC values and the exponential distribution is better without user's hand and with wider AS. Moreover, the wider ASs give less μ and are closer to zero distribution, since ECC values get smaller as the AS gets wider.

Figure 9 shows the cumulative distribution function (CDF) of ECC. The CDF curves show that user's hand increases ECC between ports for the same AS. In addition, a wider AS produces less ECC. The values of ECC corresponding to the CDF horizontal level of 0.5 are plotted in Figure 10.

With AS value of $10°$, the values of ECC at CDF = 0.5 are 0.25 and 0.37 without and with user hand, respectively. These values keep decreasing with wider AS to arrive at 0.4 and 0.07 when AS is $70°$.

6. CONCLUSION

This paper presents the calculated ECC results between two ports of a MIMO antenna operating in the sub 6 GHz band with user's hand effect. ECC was analyzed in uniform and Gaussian environments. Different AS values were used in the Gaussian environment. Results show that the maximum ECC value is less than 0.16 in a uniform APS when user hand grips the device. However, maximum ECC between ports varies significantly according to the direction of the incident wave and the width of the AS. When AS value is $10°$, the variations in ECC are from 0.16 up to 0.84 without user hand, and from 0.21 up to 0.92 with user hand. Mean ECC values of 0.25 and 0.37 are observed without and with user hand, respectively. With increased AS to $70°$, the ECC dropped from 0.04 to 0.23 (without user's hand) and from 0.04 to 0.34 (with user's hand), whereas the mean ECC values also decreased to 0.04 and 0.07 without and with user's hand, respectively. Statistically, ECCs for both cases without and with user's hand show good agreement in exponential distribution. Gaussian APS with AS of $70°$ shows similar results to uniform environment in terms of ECC values and the frequencies that produce the highest ECC. In general, analyzing the ECC of the MIMO antenna in the directive propagation environment such as Gaussian environment shows degradation in performance and fluctuations that are not observed when uniform APS is assumed. This degradation in ECC will consequently affect the performance of the MIMO antenna performance in terms of diversity combining gain and capacity.

REFERENCES

1. Kaiser, T. and F. Zheng, *Ultra Wideband Systems with MIMO*, John Wiley & Sons, 2010.

2. Rappaport, T. S., Y. Xing, G. R. MacCartney, Jr., A. F. Molisch, E. Mellios, and J. Zhang, "Overview of millimeter wave communications for fifth-generation (5G) wireless networks — With a focus on propagation models," *IEEE Trans. Antennas Propag.*, Vol. 65, No. 12, 6213–6230, 2017.

3. Zhekov, S. S., A. Tatomirescu, E. Foroozanfard, and G. F. Pedersen, "Experimental investigation on the effect of user's hand proximity on a compact ultrawideband MIMO antenna array," *IET Microwaves, Antennas Propag.*, Vol. 10, No. 13, 1402–1410, 2016.

4. Andersen, J. B., L. Fellow, J. Ø. Nielsen, and G. F. Pedersen, "Absorption related to hand-held devices in data mode," *IEEE Transactions on Electromagnetic Compatibility*, Vol. 58, No. 1, 47–53, 2016.

5. Allen, W. N. and D. Peroulis, "Bandwidth-optimal single-tunable-element matching network for antenna tuning in mobile handsets," *2011 IEEE MTT-S International Microwave Symposium Digest (MTT)*, 1–4, 2011.

6. Li, Y., Y. Luo, and G. Yang, "12-port 5G massive MIMO antenna array in sub-6 GHz mobile handset for LTE bands 42/43/46 applications," *IEEE Access*, Vol. 6, 344–354, 2018.

7. Khan, R., A. A. Al-Hadi, and P. J. Soh, "Recent advancements in user effect mitigation for mobile terminal antennas: A review," *IEEE Transactions on Electromagnetic Compatibility*, Vol. 61, No. 1, 1–9, 2018.

8. Ban, Y.-L., C. Li, G. Wu, and K.-L. Wong, "4G/5G multiple antennas for future multi-mode smartphone applications," *IEEE Access*, Vol. 4, 2981–2988, 2016.

9. Li, M.-Y., Y.-L. Ban, Z.-Q. Xu, G. Wu, K. Kang, and Z.-F. Yu, "Eight-port orthogonally dual-polarized antenna array for 5G smartphone applications," *IEEE Trans. Antennas Propag.*, Vol. 64, No. 9, 3820–3830, 2016.

10. Wong, K.-L., C.-Y. Tsai, and J.-Y. Lu, "Two asymmetrically mirrored gap-coupled loop antennas as a compact building block for eight-antenna MIMO array in the future smartphone," *IEEE Trans. Antennas Propag.*, Vol. 65, No. 4, 1765–1778, 2017.

11. Sharawi, M. S., "Current misuses and future prospects for printed multiple-input, multiple-output antenna systems," *IEEE Antennas Propag. Mag.*, Vol. 59, No. 2, 162–170, 2017.

12. Tian, R., B. K. Lau, and Z. Ying, "Multiplexing efficiency of MIMO antennas in arbitrary propagation scenarios," *2012 6th European Conference on Antennas and Propagation (EUCAP)*, 373–377, 2012.

13. Taga, T., "Analysis for mean effective gain of mobile antennas in land mobile radio environments," *IEEE Trans. Veh. Technol.*, Vol. 39, No. 2, 117–131, 1990.

14. Dong, L., H. Ling, and R. W. J. Heath, "Multiple-input multiple-output wireless communication systems using antenna pattern diversity," *IEEE Global Telecommunications Conference, 2002, GLOBECOM'02*, Vol. 1, 997–1001, 2002.

15. Pedersen, K. I., P. E. Mogensen, and B. H. Fleury, "Power azimuth spectrum in outdoor environments," *Electron. Lett.*, Vol. 33, No. 18, 1583–1584, 1997.

16. Sharawi, M. S., A. T. Hassan, and M. U. Khan, "Correlation coefficient calculations for MIMO antenna systems: A comparative study," *Int. J. Microw. Wirel. Technol.*, Vol. 9, No. 10, 1991–2004, 2017.

17. Blanch, S., J. Romeu, and I. Corbella, "Exact representation of antenna system diversity performance from input parameter description," *Electron. Lett.*, Vol. 39, No. 9, 705–707, 2003.

18. Stjernman, A., "Relationship between radiation pattern correlation and scattering matrix of lossless and lossy antennas," *Electron. Lett.*, Vol. 41, No. 12, 1, 2005.

19. Hallbjorner, P., "The significance of radiation efficiencies when using S-parameters to calculate the received signal correlation from two antennas," *IEEE Antennas Wirel. Propag. Lett.*, Vol. 4, No. 1, 97–99, 2005.

20. Vaughan, R. G. and J. B. Andersen, "Antenna diversity in mobile communications," *IEEE Trans. Veh. Technol.*, Vol. 36, No. 4, 149–172, 1987.

21. Sun, D. and C. Wei, "Analysis and design of 4×4 MIMO-antenna systems in mobile phone," *J. Comput. Commun.*, Vol. 4, No. 2, 26, 2016.

22. Tounou, C. A., C. Decroze, D. Carsenat, T. Monédière, and B. Jecko, "Mobile communication antennas in uniform and Gaussian propagation channels," *The Second European Conference on Antennas and Propagation, EuCAP 2007*, Edinburgh, UK, 2007.

23. Kyosti, P., "WINNER II channel models," *IST, Tech. Rep. IST-4-027756 Win. II D1. 1.2 V1. 2*, 2007.

24. Vasilev, I., V. Plicanic, and B. K. Lau, "Impact of antenna design on MIMO performance for compact terminals with adaptive impedance matching," *IEEE Trans. Antennas Propag.*, Vol. 64, No. 4, 1454–1465, 2016.

25. Buskgaard, E., A. Tatomirescu, S. C. Del Barrio, O. Franek, and G. F. Pedersen, "User effect on the MIMO performance of a dual antenna LTE handset," *2014 8th European Conference on Antennas and Propagation (EuCAP)*, 2006–2009, 2014.

26. Stavrou, E., H. Shakhtour, J. Pamp, and D. Heberling, "2-port antenna on fleece substrate for on-body mimo applications," *2012 6th European Conference on Antennas and Propagation (EUCAP)*, 3317–3321, 2012.

27. Malviya, L., R. K. Panigrahi, and M. V Kartikeyan, "A 2 × 2 dual-band MIMO antenna with polarization diversity for wireless applications," *Progress In Electromagnetics Research C*, Vol. 61, 91–103, 2016.

28. Ilvonen, J., R. Valkonen, J. Holopainen, and V. Viikari, "Multiband frequency reconfigurable 4G handset antenna with MIMO capability," *Progress In Electromagnetics Research*, Vol. 148, 233–243, 2014.